Molecular Vision 2016; 22:1318-1331 <http://www.molvis.org/molvis/v22/1318>
Received 11 November 2015 | Accepted 8 November 2016 | Published 10 November 2016

Genetic and immunohistochemical analysis of HSPA5 in mouse and human retinas

Sumana R. Chintalapudi,[1,2] XiaoFei Wang,[1] Huiling Li,[1,3] Yin H. Chan Lau,[1] Robert W. Williams,[2,4] Monica M. Jablonski[1,2,5]

[1]Department of Ophthalmology, Hamilton Eye Institute, The University of Tennessee Health Science Center, Memphis, TN; [2]Department of Anatomy and Neurobiology, The University of Tennessee Health Science Center, Memphis, TN; [3]Department of Ophthalmology, the Second Xiangya Hospital, Central South University, Changsha, Hunan, China; [4]Department of Genetics, Genomics and Informatics, The University of Tennessee Health Science Center, Memphis, TN; [5]Department of Pharmaceutical Sciences, The University of Tennessee Health Science Center, Memphis, TN

Purpose: Photoreceptor degenerative diseases are among the leading causes of vision loss. Although the causative genetic mutations are often known, mechanisms leading to photoreceptor degeneration remain poorly defined. We have previously demonstrated that the photoreceptor membrane-associated protein XAP-1 antigen is a product of the *HSPA5* gene. In this study, we used systems genetic methods, statistical modeling, and immunostaining to identify and analyze candidate genes that modulate Hspa5 expression in the retina.

Methods: Quantitative trait locus (QTL) mapping was used to map the genomic region that regulates *Hspa5* in the cross between C57BL/6J X DBA/2J mice (BXD) genetic reference panel. The stepwise refinement of candidate genes was based on expression QTL mapping, gene expression correlation analyses (direct and partial), and analysis of regional sequence variants. The subcellular localization of candidate proteins and HSPA5 in mouse and human retinas was evaluated by immunohistochemistry. Differences in the localization of extracellular HSPA5 were assessed between healthy human donor and atrophic age-related macular degeneration (AMD) donor eyes.

Results: In the eyes of healthy mice, extracellular HSPA5 was confined to the area around the cone photoreceptor outer segments. Mapping variation in *Hspa5* mRNA expression levels in the retina revealed a statistically significant *trans*-acting expression QTL (eQTL) on Chromosome 2 (Chr 2) and a suggestive locus on Chr 15. *Sulf2* on Chr 2 was the strongest candidate gene based on partial correlation analysis, Pearson correlation with *Hspa5*, expression levels in the retina, a missense variant in exon 14, and its reported function in the extracellular matrix and interphotoreceptor matrix. SULF2 is localized to the rod and cone photoreceptors in both human and mouse retinas. In human retinas with no pathology, extracellular HSPA5 was localized around many cones within the macular area. In contrast, fewer HSPA5-immunopositive cones were observed in the retinas from AMD donors.

Conclusions: We identified *Sulf2* as a candidate gene modulating the *Hspa5* expression in the retina. The preferential loss of HSPA5 in the interphotoreceptor matrix around cone photoreceptors in atrophic AMD retinas opens up new avenues for exploring the changes in interphotoreceptor matrix (IPM) that are associated with macular disease.

Heat shock proteins protect and maintain cell viability primarily by acting as molecular chaperones under stressful conditions [1]. HSPA5 (GRP78, also known as binding immunoglobulin protein [BiP]) is a well-established endoplasmic reticulum (ER) chaperone. It is involved in many cellular processes, including the translocation of newly synthesized polypeptides across the ER membrane, facilitating the folding and assembly of proteins, targeting misfolded proteins for ER-associated protein degradation, regulating calcium homeostasis, and serving as an ER stress sensor [2-5]. An upregulation of HSPA5 is an indication of ER stress in various mouse models of retinal degeneration, such as light-induced retinal degeneration [6], the *rd1* mouse [7], and retinal detachment [8].

In addition to being an ER resident protein, HSPA5 has also been characterized as a soluble protein localized to the interphotoreceptor matrix (IPM) surrounding the cones in pig and mouse retinas and to the IPM surrounding both rods and cones in *Xenopus laevis* [9-11]. Previously, our laboratory identified the *Xenopus* Anti-Photoreceptor-1 (XAP-1) antigen as the extracellular form of HSPA5 [10]. Interestingly, we discovered that in the absence of RPE, HSPA5 was no longer present in the IPM surrounding the photoreceptor outer segments. Moreover, the outer segments were improperly folded in RPE-deprived explanted *Xenopus* retinas. Of possible physiologic importance, HSPA5 immunopositive labeling in the IPM was detectable in a pattern similar to that of the control after the addition of a neuro-supportive

Correspondence to: Monica Jablosnki, The University of Tennessee Health Science Center, Hamilton Eye Institute, 930 Madison Avenue, Suite 758, Memphis, TN 38163, Phone: (901) 448 7572; FAX: (901) 448 5028; email: mjablonski@uthsc.edu

agent [12]. Although we demonstrated a clear correlation between the presence of HSPA5 in the IPM and the proper outer segment ultrastructure, the role of the extracellular form of HSPA5 in photoreceptor health or degeneration remains unknown.

Systems genetics integrates and interprets high-throughput quantitative molecular data to model cellular responses and disease outcomes using a genetic reference population [13-16], such as the BXD family of advanced crosses, which is the largest and best-characterized murine genetic reference population available. These strains were generated by crossing two widely used inbred strains of mice: C57BL/6J (B6) and DBA2/J (D2) [17,18]. Most molecular and genetic data for the BXD family has been archived in the GeneNetwork, including many datasets that are relevant to the genetics and genomics of the eye and central visual system [19-23].

The purpose of this investigation was to identify the genes that modulate the expression of Hspa5 in the mouse retina. A secondary goal was to determine the localization pattern of HSPA5 in healthy and diseased human retinas. In this study, we used various systems genetics methods and ex vivo studies to identify *Sulf2* as the best candidate gene to modulate the expression of Hspa5 in the retina. HSPA5 is confined to the IPM surrounding the cone photoreceptors in human donor eyes that have no ocular pathology, yet it is nearly absent in atrophic age-related macular degeneration (AMD) eyes. We hypothesized that Hspa5 may play an important role in maintaining cone photoreceptor structural integrity, and that its expression was modulated by *Sulf2*.

METHODS

Mice: This study was approved by The Animal Care and Use Committee at The University of Tennessee Health Science Center (UTHSC). Mice were handled in a manner consistent with the ARVO Statement for the Use of Animals in Ophthalmic and Vision Research and the Guide for the Care and Use of Laboratory Animals (Institute of Laboratory Animal Resources, Public Health Service Policy on Humane Care and Use of Laboratory Animals). A total of 80 strains (n = 326) of BXD mice from both sexes were used for the systems genetics study. Three BXD100 mice (2 months old, including both sexes) were used in the immunohistochemistry study. No abnormal phenotypes were detected in the eyes of these mice. More importantly, they lacked the pigmentary dispersion phenotype that is present in DBA/2J mice. The animals were maintained on a 12 h: 12 h light-dark cycle, at a temperature from 20 °C to 24 °C and were allowed food and water ad libitum.

Human tissue: Our research and protocol for the collection of human retinas was conducted in accordance with the tenets of the Declaration of Helsinki and approved by University of Tennessee Health Science Center Institutional Review Board (IRB). The control donor eyes had no history of eye disease; the age and sex of the donors were 47 years (M), 59 years (F), 69 years (F), 77 years (F), 87 years (M), and 93 years (M). The age-matched human donor eyes had a clinical diagnosis of atrophic AMD; the age and sex of the donors were70 years (M), 79 years (M), 87 years (M), and 94 years (F). All eyes were obtained from the Mid South Eye Bank and the Lions Eye Bank of Oregon. All eyes were procured and processed in compliance with the Medical Standards of the Eye Bank Association of America (EBAA) and Government regulations. Eyes were fixed within 5 h of death in formalin solution. Anterior segment structures were removed and the fundus was photographed. The clinical diagnosis of each eye was confirmed by an ophthalmologist. Full thickness biopsies of the macula region centered on the fovea, and the far peripheral temporal retinas of each eye were removed with a 6-mm diameter punch (Miltex, York, PA).

Immunofluorescence staining: To obtain the light level immunolocalization of the antigens of interest, the mouse and human retinas were embedded in low molecular weight agarose and sectioned at a thickness of 50 µm. Immunofluorescence staining for both intracellular and extracellular HSPA5 was performed according to our previously published protocol. Briefly, tissue sections were blocked with 10% goat serum and permeabilized with 0.1% Triton X-100 or left un-permeabilized to differentiate intracellular and extracellular localization patterns, respectively based on our previously published protocol [10]. Tissue sections were then either labeled with anti-XAP-1 (HSPA5; Clone 3D2, monoclonal antibody, Developmental Studies Hybridoma Bank, University of Iowa, IA, 1:1 dilution) or anti-sulfatase 2 antibody (SULF2; rabbit polyclonal IgG, Santa Cruz Biotechnology, Dallas TX, 1:200 dilution). This was followed by Alexa Fluor 488 or 568-conjugated secondary antibody (Invitrogen, Carlsbad, CA; 1:200 dilution) to detect the antigen of interest. Peanut agglutinin (PNA)-tagged with Alexa Fluor 488 or 568 (Molecular Probes, Eugene, OR; 1:25 dilution) and wheat germ agglutinin (WGA)-tagged with Alexa Fluor 633 (Molecular Probes; 1:50 dilution) were used to differentiate the cone and rod photoreceptors, respectively. TO-PRO3 iodide (1:4000 dilution; Invitrogen) was used to label the nuclei. Sections were viewed and images were obtained using a Nikon C1 confocal microscope within the Imaging Core Facility in the Hamilton Eye Institute. All microscope settings, including laser levels and gain, were held constant to

allow for relative comparisons of signal intensity within and between experiments.

Electron microscopic (EM) immunohistochemical analyses were performed using our previously published protocol [12]. Briefly, formalin fixed human donor eyes were embedded in LR White (Electron Microscopy Sciences, Hatfield, PA). Ultra-thin sections were collected on mesh nickel grids. The sections were blocked with 10% normal goat serum (Vector Laboratories, Burlingame, CA) and incubated in anti-XAP1 antibody (1:1 dilution) at 4 °C overnight, followed by incubation with a gold-conjugated secondary antibody (1:10 dilution, 10 nm gold particles; Sigma-Aldrich, St. Louis, MO). Sections were washed and images were captured with an electron microscope (JEM 200EX II; JEOL, Tokyo, Japan).

HEI retina database: The Hamilton Eye Institute (HEI) Retina Database contains the data analysis of 346 Illumina Sentrix® Mouse Whole Genome-6 version 2.0 arrays (Illumina, San Diego, CA). This database contains the retinal transcriptome profiles of 80 strains of BXD mice aged between 2 and 4 months. We used the Normal HEI Retina dataset available on the GeneNetwork to perform QTL analysis and define genetic networks. These data are globally normalized to produce arrays that have a mean of 8 and a standard deviation of 2 [23,24].

Expression QTL (eQTL) mapping and heritability calculation: On the Illumina array, *Hspa5* is represented by a single probe set (ILMN_1255561) that hybridizes to the proximal 3′ untranslated region (UTR) of *Hspa5* on Chromosome 2 (Chr 2) at 34.631669 Mb on the plus strand. The eQTL mapping was performed using our previously published methods [19,21].

QTL mapping was carried out using the WebQTL module available in GeneNetwork. Simple interval mapping was performed at regular intervals to identify eQTLs that regulate *Hspa5* expression. The level of significance was estimated by permutations analyses. Mapping analyses produced a likelihood ratio statistic (LRS) score, providing us with a measure of the strength of linkage between *Hspa5* expression level variation and genotype markers.

Evaluation of candidate genes: partial correlation, heat map analyses and SNP identification: Using the tools available on the GeneNetwork, partial correlation analyses were performed using our previously published methods [25-28]. In the current study, the partial correlation feature on the GeneNetwork was used to identify a candidate gene that modulates Hspa*5* expression in the retina. A partial correlation is defined as the relationship between a primary variable and a target variable after the influence of one or more related variables are removed [27]. In this case, the expression of *Hspa5* was the primary variable and the expression levels of the candidate regulatory genes within the retina database were the target variables. The *trans*-effect of the eQTL on Chr 2 was mathematically controlled using the markers rs3143843 (Chr 2: 169.778380) and rs3673248 (Chr 2: 172.849974), which straddle the *trans*-eQTL to strengthen the relationship between the *Hspa5* expression and the potential candidate genes. Using the partial correlation function, we generated the top 100 gene correlates of *Hspa5*. To evaluate the relationship between *Hspa5* and the QTL region, this list of 100 correlates was analyzed by constructing a heat map in which the more intense colors indicated the chromosomal regions with comparatively high linkage statistics. The top candidate genes with a biologic function or a localization pattern associated with the extracellular or interphotoreceptor matrix were selected for further analyses.

The Pearson correlation coefficients with *Hspa5* were calculated for the candidate genes using the tools available in the GeneNetwork. Candidate genes with significant Pearson correlation (threshold≥0.5) values with *Hspa5* were examined for the presence of non-synonymous single nucleotide polymorphisms (SNPs) or insertions and deletions (InDels). A detailed list of polymorphisms between the D2 and B6 parental strains is freely available on the GeneNetwork and the original sequence data are available at 327618. A second heat map that included only the candidate modulatory genes was also generated to evaluate their relationship with *Hspa5*. All correlation values for candidate gene prioritization were adjusted for multiple comparisons using the Bonferroni correction.

RESULTS

Expression pattern of extracellular HSPA5 in mouse retinas: Previously, we determined that the XAP-1 antibody labels extracellular HSPA5 in *Xenopus* retinas [10,12]. To determine which cell types in the mouse retina were labeled by the HSPA5 antibody, we performed immunohistochemical analysis. In mouse retinas, HSPA5 preferentially co-localized with PNA around the cone photoreceptors. A minor amount of HSPA5 was co-localized with WGA around the rods (Figure 1A-D). To differentiate between extracellular and intercellular HSPA5, mouse retina sections were un-permeabilized or permeabilized, respectively, before immunohistochemistry was performed. In the non-permeabilized tissue, intense HSPA5 immunolabeling co-localized with PNA, which indicated that extracellular HSPA5 expression was predominantly present in the IPM surrounding the cone photoreceptors

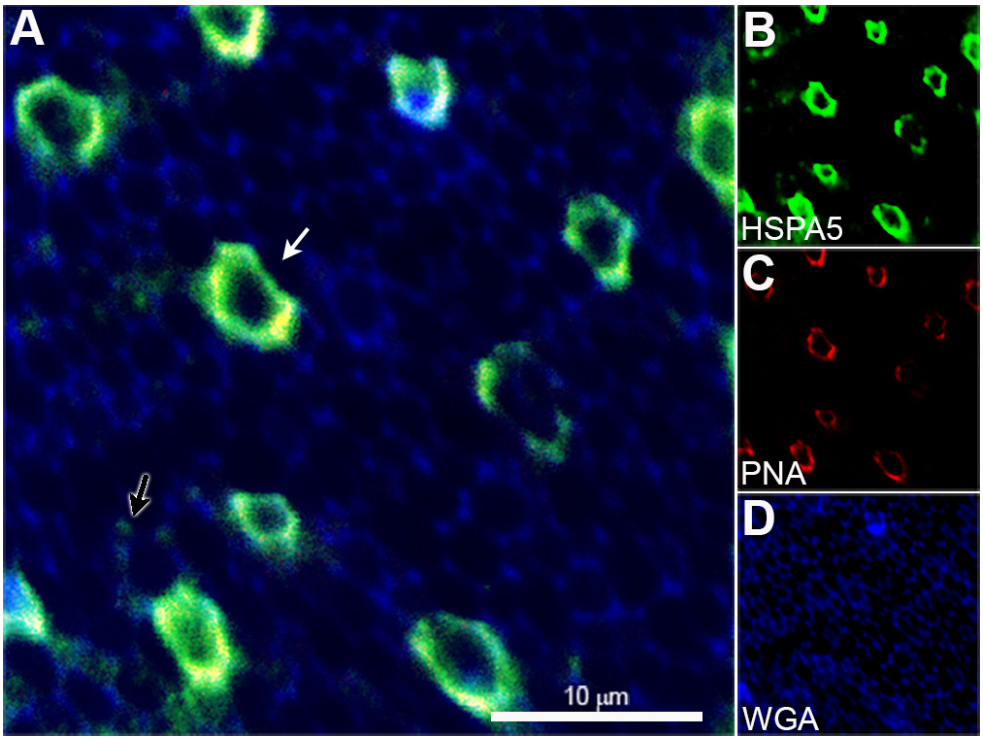

Figure 1. Immunohistochemical localization of HSPA5 in mice retinas (en face presentation). **A-D**: HSPA5 (green) co-localizes with PNA (red) in the IPM surrounding the cone photoreceptors. The co-localization of HSPA5 and PNA is shown in yellow (white arrow). A minimal amount of HSPA5 immunolabeling is associated with WGA around rods (black arrow). Binding of WGA to the IPM surrounding the rods is shown in blue. Scale bar = 10 µm.

(Figure 2A-D). After permeabilization, a similar pattern of extracellular HSPA5 localization was observed in the IPM surrounding the cone photoreceptors (Figure 2E-H). No intracellular labeling was detected using the XAP-1 antibody.

Bioinformatic analyses of Hspa5: Using the HEI retina database available on the GeneNetwork, we determined that there was a significant variation in the level of *Hspa5* transcript in the retina across the BXD strains (Figure 3A). The average expression level of *Hspa5* was 7.6±0.0 and the range was 6.9±0.2 (BXD80) to 8.4±0.3 (BXD102). Simple interval mapping for *Hspa5* revealed a significant *trans*-eQTL with the likelihood ratio statistics (LRS) of 18.4 (genome wide significance at $p \leq 0.05$) on Chr 2 with a peak between 170 and 173 Mb. A suggestive peak on Chr 15 between 85 and 90 Mb with an LRS of 14.3 was also observed (Figure 3B).

Candidate gene selection: To identify the candidate genes that could modulate the expression of *Hspa5* in the retina, we performed a partial correlation analysis within the GeneNetwork. By mathematically controlling for the QTL on the Chr 2 peak, we generated a list of the top 2,000 correlates of *Hspa5*. To select the top candidate genes within this list that modulated the variation in the expression of *Hspa5* in the retina, we used the following criteria:

• The gene was expressed in the retina;

• The gene was located within 5 Mb of the QTL peaks on Chr 2 and Chr 15 that were identified using simple interval mapping;

• The expression of the gene exhibited a high (≥0.5) correlation with *Hspa5*; and

• The gene had functional relevance to the extracellular matrix, including the IPM.

Of the 71 genes residing within the *trans*-eQTLs on Chr 2 and Chr 15, the following genes fulfilled the selection criteria: *Dpm1* and *Sulf2* (located in the *trans*-eQTL interval on Chr 2), and *Fbln1*, *Glt8d3*, and *Pmm1* (located in the eQTL interval on Chr 15). Table 1 provides the details of each gene.

By performing a direct Pearson correlation calculation between the variation in the levels of *Hspa5* and that of the six candidate genes, we determined that the variation in the levels of *Sulf2*, *Pmm1*, and *Fbln1* had very high correlation coefficients of 0.775 (Adjusted [adj]. $p = 6.0\times10^{-16}$), −0.725 (adj. $p = 1.7\times10^{-12}$), and 0.611 (adj. $p = 4.4\times10^{-08}$), respectively, with variation in the expression of *Hspa5*. Variation of *B4galt5*, *Dpm1*, and *Glt8d3* had moderate correlation coefficients of 0.486 (adj. $p = 6.9\times10^{-05}$), −0.486 (adj. $p = 6.6\times10^{-0.5}$), and 0.493 (adj. $p = 4.8\times10^{-05}$), respectively, with variation in the level of *Hspa5*.

A heat map that was generated using the top 100 transcripts with the highest Pearson correlation coefficients

with *Hspa5* revealed tight bands on Chr 2 and Chr 15 at the location of the QTL peaks found when mapping the *Hspa5* expression (Figure 4A). A second heat map generated with only *Hspa5* and the six candidate genes had a banding pattern similar to the heat map for the top 100 transcripts (Figure 4B). These data indicated that both groups of genes shared common signature QTLs, which suggested that they were all part of the same genetic signature network.

To further evaluate the strength of these six candidate genes, we determined if there were any sequence variants between the parental strains. The data in the UCSC Genome Browser on Mouse Assembly (UCSC mm9, July 2007) showed no missense/nonsense SNPs in *B4galt5*, *Dpm1*, *Fbln1*, *Glt8d3*, or *Pmm1*. One non-synonymous SNP was present in *Sulf2* in exon 14 (Table 1). The SNP in *Sulf2* resulted in a change in the amino acid sequence in which an arginine was replaced by a lysine, which can lead to the synthesis of an altered protein product (Table 1). Only *Sulf2* met all of the criteria for the selection of a candidate gene.

Expression pattern of SULF2 in mouse retinas: To strengthen *Sulf2* as a candidate gene modifier of *Hspa5*, we analyzed the localization pattern of SULF2 by immunofluorescence in cross sections of mouse retinas. In the tissue lacking permeabilization, SULF2 was predominantly present in the extracellular space around the cone outer segments (OS; Figure 5A-D), which demonstrated that a small amount of secreted SULF2 was present in the IPM around the cone photoreceptors. After tissue permeabilization, an intense immunoreactivity for SULF2 was observed in the outer nuclear layer (ONL), as well as around the inner segments (IS) and OS of the cone photoreceptors (Figure 5E-H). A similar pattern was detected in the normal human donor retina sections (Figure 5I-P, representative image).

Expression pattern of HSPA5 in retinas from human donor eyes: In our previously published study, we determined that HSPA5 was associated with the IPM surrounding the rod and cone photoreceptors in *Xenopus laevis* retinas [12]. However, in mouse retinas, extracellular HSPA5 was preferentially localized to the cone photoreceptors [10] (Figure 1 and Figure 2). Building on this observation, we sought to determine if the localization pattern of extracellular HSPA5 was conserved in mammals, and if macular disease affected the presentation of

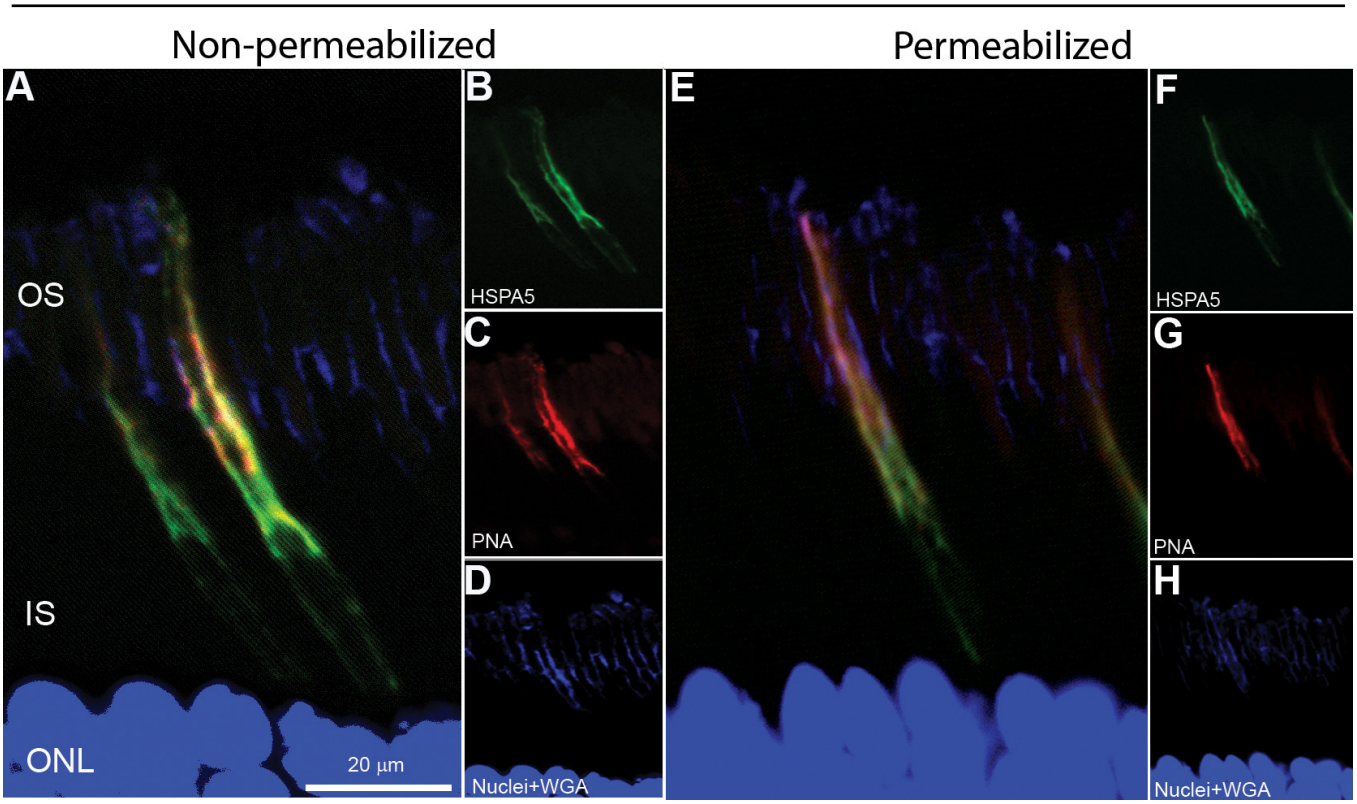

Figure 2. Localization of intracellular and extracellular HSPA5 in retina cross sections from mice. **A-D**: In non-permeabilized sections, HSPA5 (green) co-localizes with PNA (red) in the IPM surrounding the cone photoreceptors. The co-localization of HSPA5 and PNA is shown in yellow. **E-H**: In permeabilized retina cross sections, HSPA5 co-localizes with PNA in a pattern similar to the non-permeabilized retina cross sections (yellow). OS = outer segments, IN = inner segments, ONL = outer nuclear layer. Scale bar = 20 µm.

HSPA5. In human donor retinas from eyes with no pathology, intense HSPA5 expression was co-localized with PNA in the macula (Figure 6A-D). This indicated that in the human retina, HSPA5 immunolabeling was more abundant in the IPM surrounding the cone photoreceptors than in the IPM surrounding the rod photoreceptors. The cross sectional view of the macular retina showed the HSPA5 expression around the cone photoreceptors along the entire IPM (Figure 6E-H). The results were representative of all the donor eyes.

To better characterize the localization of HSPA5 in human retinas, we performed an EM immunolocalization analysis. At the EM level, HSPA5 was preferentially associated with flocculent material on the surface of the plasma membrane of the cone photoreceptors. In contrast, there was minimal immunolabeling around the rod photoreceptors (Figure 6I,J).

In ocular diseases, such as age-related macular degeneration, the primary cellular target leading to vision loss is the cone photoreceptors. To compare the localization pattern

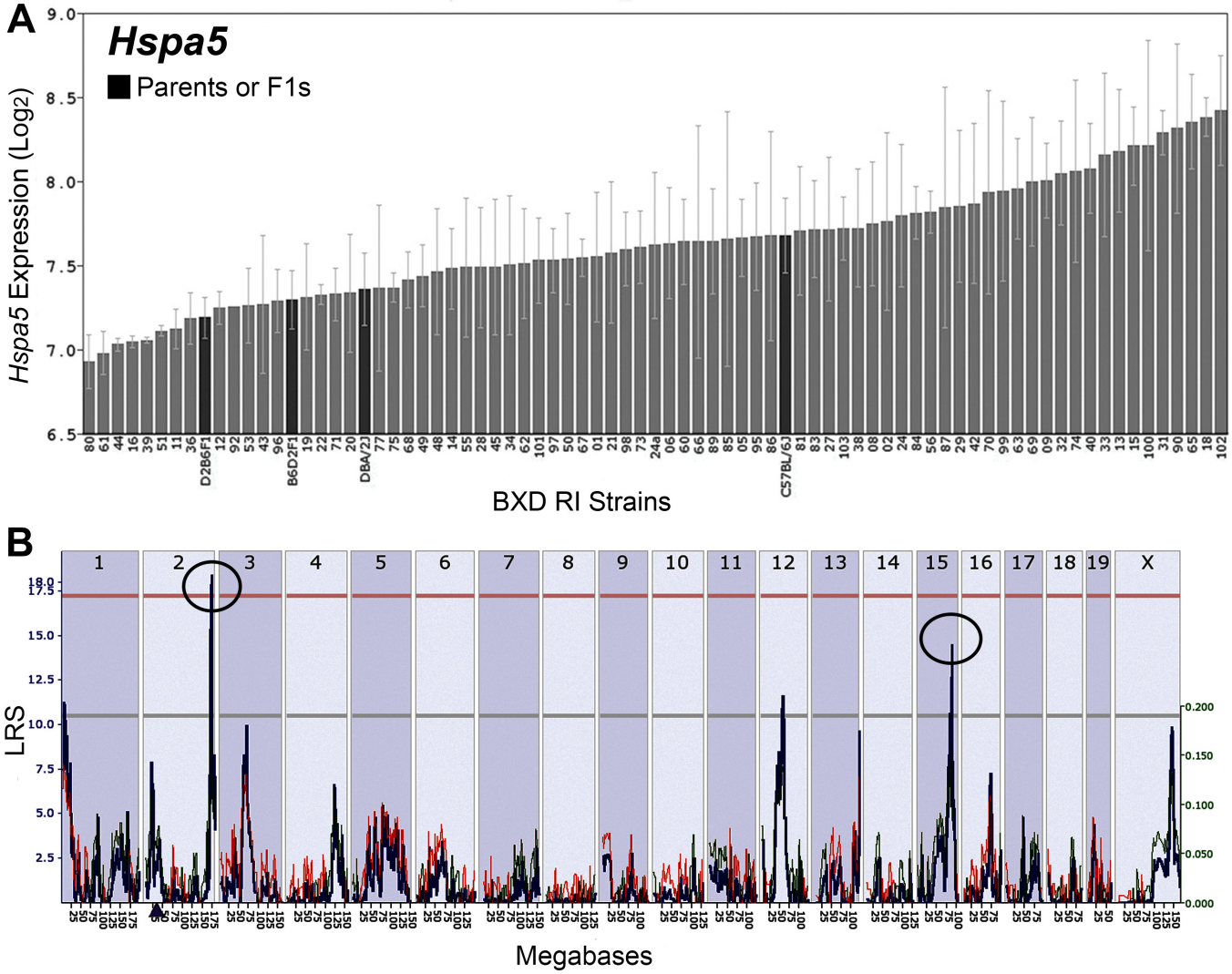

Figure 3. Expression levels of *Hspa5* across the BXD strains and simple interval mapping. **A**: Rank-ordered mean *Hspa5* levels across the BXD recombinant inbred family ranges from 6.9±0.2 in BXD80 to 8.4±0.3 in BXD102. The values denote the normalized relative expression levels on a $\log_2$ scale (mean±SEM). **B**: The QTL simple interval map of genomic regions that modulate *Hspa5* expression in the retinas of BXD mice. A significant *trans*-eQTL for *Hspa5* is present on Chr 2 and a second *trans*-eQTL is present on Chr 15 (circles). The blue tracings indicate the LRS scores across the genome. The *x*-axis represents the LRS scores across the genome. The horizontal lines represent the transcript-specific significance thresholds for significant (LRS = 17.21) and suggestive (LRS = 10.48) LRS levels indicated by red and gray horizontal lines, respectively. The filled triangle on Chr 2 indicates the location of *Hspa5* in the genome.

Table 1. Summary of candidate genes.

Gene I.D.	Location	Max LRS value and Location	Probe set I.D. and BLAT specificity	Markers flanking the gene	Mean expression level	SNPs and Indels
Hspa5	Chr2: 34,772,090-34776529 bp	18.3; Chr2:172.56 Mb	ILMN_1255561; 2.6	rs13476425	7.614	• Two transcript variants
Sulf2	Chr2: 34,772,090-34776529 bp	20.6; Chr15: 87.93 Mb	ILMN_1234624; 3.1	rs13476894	7.525	• Three transcript variants • One non-synonymous SNP in exon 14 • One each synonymous SNP in exon 4 and exon 12 • 156 SNPs • 46 insertions/ deletions
B4galt5	Chr2: 167,298,445-167349178 bp	14.9; ChrX: 143.40 Mb	ILMN_1220235; 2.2	rs6219107	7.052	• One SNP at a nonsplice site • Two insertion/deletion
Dpm1	Chr2: 168,209,048-168230379 bp	19.5; Chr5: 104.57 Mb	ILMN_2590054; 2.9	rs3708726	9.397	-
Fbln1	Chr15: 85,115,885-85115935 bp	26.0; Chr15: 82.94 Mb	ILMN_2602770; 2.2	rs6357520	7.534	• Three each synonymous SNP in exons 4,5 and 15 • 452 SNPs • 77 insertions/ deletions
Glt8d3	Chr15: 93,239,742-93275084 bp	26.8; Chr15: 94.14 Mb	ILMN_2895067; 2.6	rs13482715	8.380	• One synonymous SNP at exon 5 • 78 SNPs • 21 insertions/ deletions
Pmm1	Chr15: 81,951,106-81960867 bp	34.6; Chr15: 81.65 Mb	ILMN_2611027; 2.8	rs6276391	12.317	• Two synonymous SNPs each in exons 2 and 8 • 15 SNPs • Eight insertions/ deletions

of HSPA5 in photoreceptors from human donor eyes with no pathology and age-matched human donor eyes with a diagnosis of atrophic AMD, immunohistochemistry was performed on retinal punches obtained from the macular and peripheral regions. The en face images represented the staining pattern from all the donor eyes used in the study. In the macula of the normal human donor retinas, HSPA5 was present in abundance surrounding the cones, but was detected at low levels around the rod photoreceptors (Figure 7A-C). In contrast, HSPA5-positive cones were less frequent throughout the peripheral retina (Figure 7D-F) in eyes with no ocular pathology. Atrophic AMD donor retinas exhibited an aberrant immunolabeling pattern in which there were very few HSPA5 immunopositive cells in both the macular (Figure 7G-I) and peripheral areas (Figure 7J-L) compared with that of retinas from the age-matched control eyes.

DISCUSSION

In this investigation, we confirmed that extracellular HSPA5 was a cone photoreceptor-specific marker in mouse retinas. It was also a cone marker in the macula of human donor eyes that lacked AMD-like pathology. In contrast, HSPA5 immunolabeling was drastically reduced in the donor eyes from atrophic AMD patients. We also integrated a novel application of expression genetics with biochemical analysis to dissect the molecular pathways, and identified *Sulf2* as a candidate gene that modulated *Hspa5* expression in the retina.

A major cause of adult blindness in developed countries is the progressive dysfunction and death of retinal photoreceptors. Photoreceptors are structurally unique photosensitive cells of the neural retina [29]. The extracellular space between the photoreceptors of the retina and the apical surface of the retinal pigment epithelium is occupied by the IPM [30]. Research has demonstrated that some of the soluble and insoluble components of the IPM may contribute

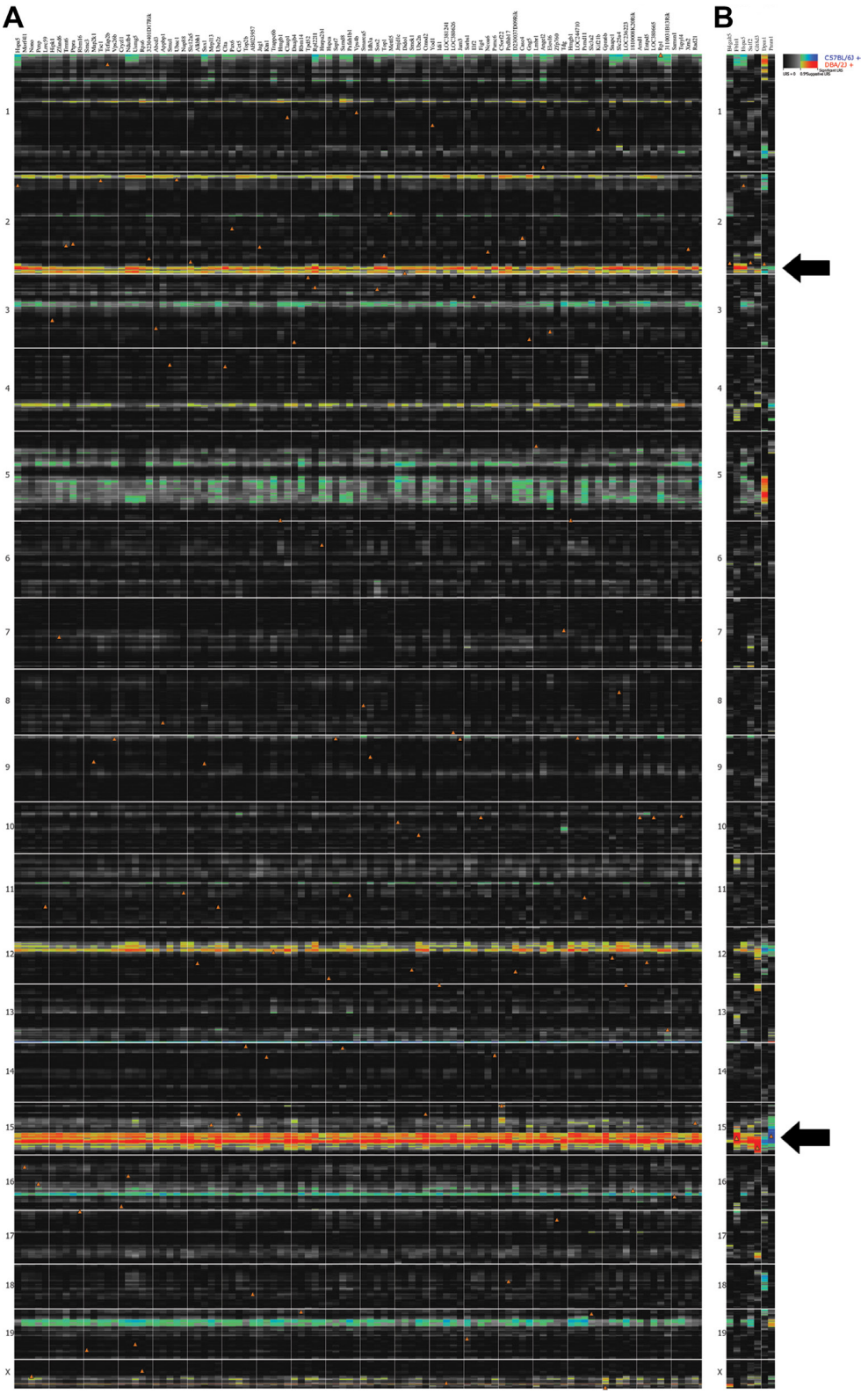

Figure 4. Heat map analysis of *Hspa5* covariates and candidate genes. **A**: Heat map of the top 100 covariates of *Hspa5* as determined by the Pearson correlation analysis. Probe sets for the various genes represent columns and the genomic location for each chromosome represents rows. Tight bands of correlates are present on Chr 2 and Chr 15 at the location of the QTL peaks, which were revealed by simple interval mapping. **B**: Heat map containing *B4galt5*, *Dpm1*, *Fbln1*, *Glt8d3*, *Sulf2*, *Pmm1*, and *Hspa5*. The hue intensity indicates the strength of the association between gene expression and genomic location. The red and blue colors indicate that the D or B allele increases trait values, respectively. The orange triangles show the location of each gene on the chromosomes. *B4galt5*, *Dpm1*, *Fbln1*, *Glt8d3*, *Sulf2*, and *Pmm1* show a strong consistency of genetic regulation across mRNA regions on Chr 2 and Chr 15 (arrows).

to visual pigment chromophore exchange, retinal adhesion, metabolite trafficking, and growth factor presentation [31-33]. Because this matrix resides in a key location and is putatively crucial in supporting photoreceptor function, documenting its structure and its components, and understanding the gene products found in the IPM can lead us closer to identifying the causes of photoreceptor degeneration.

HSPA5 is a central regulator of ER homeostasis due to its multiple functional roles in protein folding, ER calcium binding, and controlling the activation of transmembrane ER stress sensors. ER stress induction of HSPA5 represents a major pro-survival arm of the unfolded protein response (UPR). Most neurodegenerative disorders, including Parkinson's disease, Alzheimer's diseases, and progressive retinal degeneration, are characterized by the activation of the UPR and the modified expression of HSPA5 [6,7,34-36]. However, the function played by the extracellular form of HSPA5 in photoreceptor degeneration is unknown.

In the current study, we used immunohistochemistry and the XAP-1 antibody to demonstrate that extracellular HSPA5 binds to the IPM surrounding the cone photoreceptors both with and without tissue permeabilization. We confirmed that the antibody was specific for extracellular HSPA5 in mouse and human retinas. The presence of HSPA5 in the IPM around the cones in healthy human retinas and its near absence in atrophic AMD retinas suggested that HSPA5 might play a role in the cone structural integrity in the macula. However, additional studies to target the disruption of Hspa5 synthesis are required to confirm this hypothesis.

To determine which candidate genes modulate *Hspa5* transcript variation, we performed simple interval mapping. Our mapping studies in BXD mice indicated a single highly

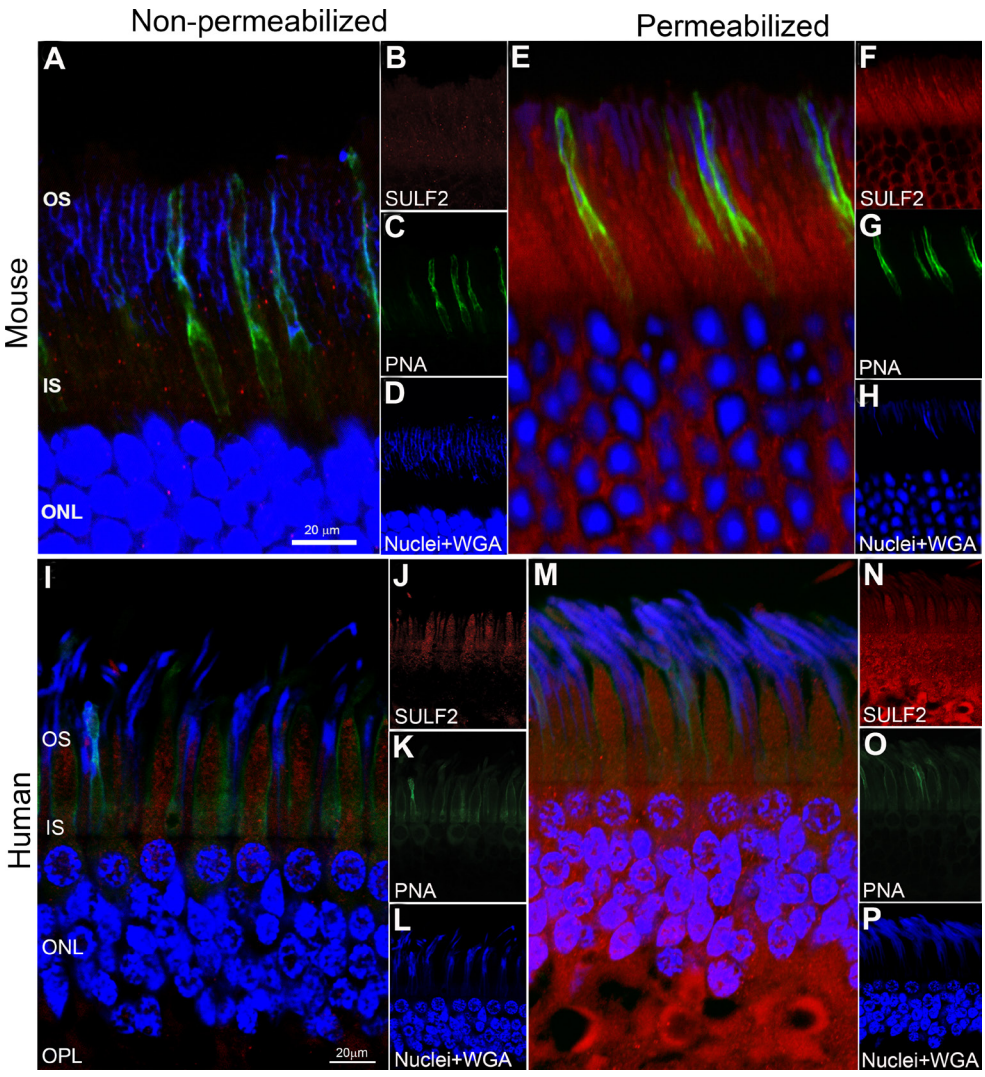

Figure 5. Immunohistochemical detection of SULF2 in non-pathological mouse and human donor retina cross sections. **A-D**: In non-permeabilized mouse retina cross sections, SULF2 (red) is observed in the extracellular space around the photoreceptor inner and outer segments. **E-H**: In permeabilized mouse retina cross sections, SULF2 (red) is predominantly observed intracellularly in the rod (blue) and cone (green) photoreceptors, as well as in the cell bodies. **I-L**: In non-permeabilized non-pathological human retina cross sections, the labeling pattern of SULF2 (red) is identical to that observed in mice. **M-P**: In permeabilized human retina cross sections, the SULF2 (red) labeling pattern is also identical to that observed in mice. OS = outer segments, IN = inner segments, ONL = outer nuclear layer, OPL = outer plexiform layer. Scale bar = 20 µm.

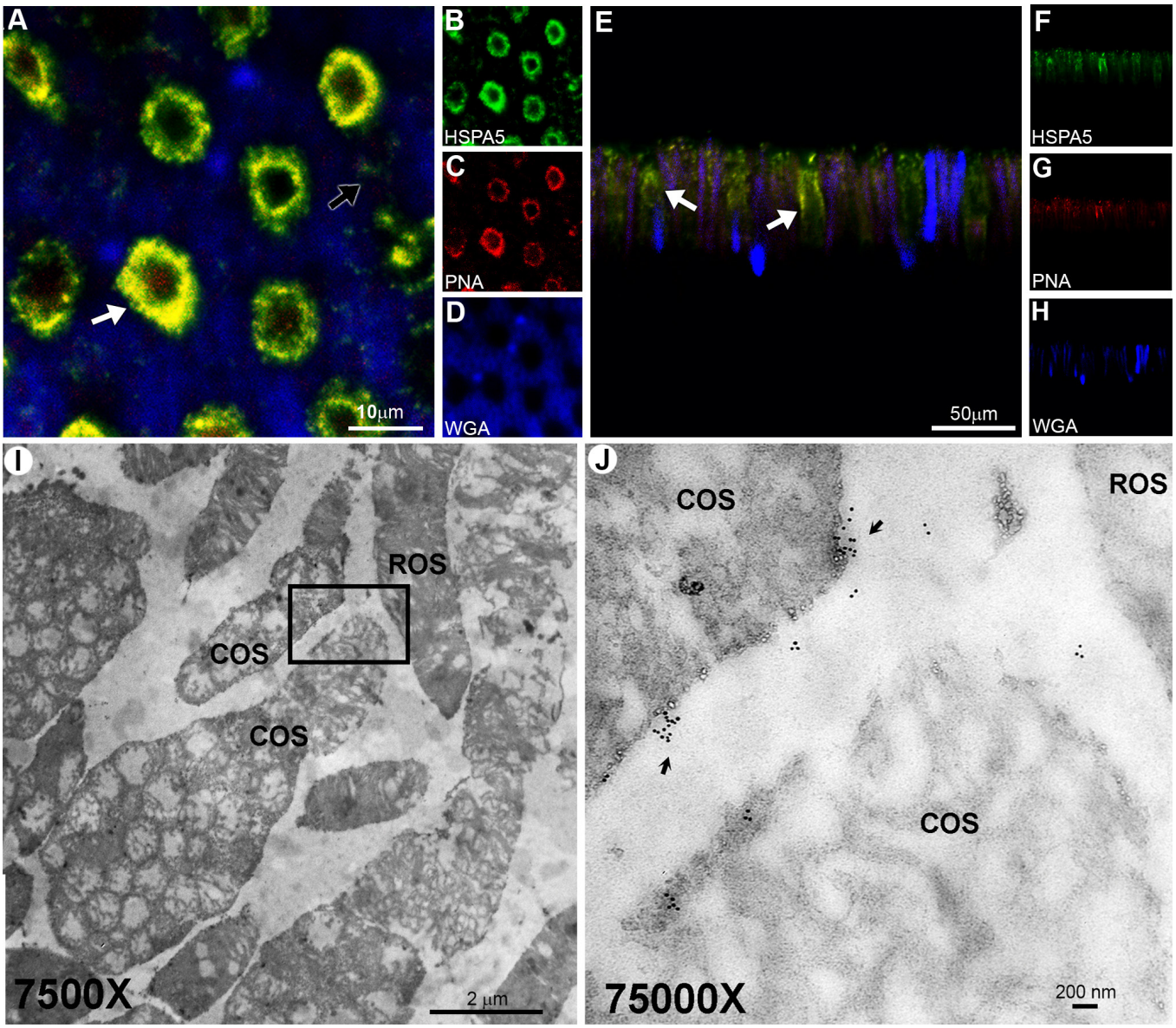

Figure 6. HSPA5 co-localizes with PNA in flat mounts and cross sections of the human macula with no pathology. **A-D**: In retinal flat mounts, HSPA5 (green) co-localizes with PNA (red). Punctate yellow indicates co-localization of HSPA5 and PNA in the IPM of the cone photoreceptors (white arrow). WGA (blue) indicates the IPM of the rods (black arrow). **E-H**: In retina cross sections, HSPA5 (green) also co-localizes with PNA along the full length of the cones (red, white arrows). WGA (blue) indicates the IPM of the rods. Scale bar = 10 μm. Electron microscopic immunohistochemical localization of HSPA5 (gold particles) in human retinas (with no ocular pathology). **I**: HSPA5 is localized to the flocculent material in the IPM surrounding the cone outer segments between adjacent cone and rod outer segments (box). Scale bar = 2 μm. **J**: Higher magnification view of HSPA5 localization (black arrow; the boxed area in G is shown magnified in H). COS = cone outer segment, CIS = cone inner segment, and ROS = rod outer segment. Scale bar = 200 nm. Images are representative of all the donor eyes that were used in the study.

genome wide significant *trans*-eQTL on Chr 2 and a suggestive genome wide *trans*-eQTL on Chr 15, both of which suggested that *Hspa5* expression was modulated, either directly or indirectly, by a different gene in the retina. We pursued a parallel strategy of heat map analyses and partial correlation analyses to corroborate the findings of our QTL analysis for Chr 2 and 15. Our results suggested that one or more transcripts that predominantly regulate Hspa5 in a *trans* manner resided within these strong eQTLs. We focused on six positional and biologically relevant genes, *B4galt5*, *Dpm1*, *Sulf2*, *Fbln1*, *Glt8d3*, and *Pmm1*, located on Chr 2 and Chr 15 under the QTL peaks. All of these genes have been shown

to play key roles in proteoglycan maintenance and cellular signaling in extracellular matrices [37-42]. Of the six genes, only *Sulf2* had a non-synonymous SNP in the mouse genome. Interestingly, a recent genome wide association study by the AMD Gene Consortium revealed 19 AMD loci, one of which showed enrichment for genes involved in extracellular matrix remodeling [43]. This provided further evidence to support our assertion that genes modulating IPM structure or function may contribute to the pathogenesis of photoreceptor degeneration in AMD.

SULF2 is an extracellular neutral-pH sulfatase. It provides a post-synthetic mechanism for the regulation of heparan sulfate proteoglycan (HSPG) function by removing 6-O-sulfate groups from the HSPG. SULF2 can thereby modulate the signaling pathways in the retina associated with Wnt-dependent signaling [44], as well as the activities of the glial cell line-derived neurotrophic factor (GDNF) [45], sonic hedgehog (SHH) [46], vascular endothelial growth factor (VEGF) [47], fibroblast growth factor 2 (FGF2) [48], and Noggin [49].

Our immunohistochemistry data demonstrated that secreted SULF2 was present in the extracellular space surrounding the cone inner and outer segments. This expression pattern raised the possibility that the secreted form of SULF2 binds to the IPM surrounding the cone inner and outer segments. An interesting implication of this observation is that the SULF2 may regulate heat shock protein signaling in the cone photoreceptors, although the mechanism is not known.

The loss of HSPA5 around the cone photoreceptors in atrophic AMD retinas provides new avenues for exploring the changes in IPM that accompany cone photoreceptor degeneration. Because HSPA5 binds to the IPM surrounding the cone photoreceptors in human retinas, it may be important in

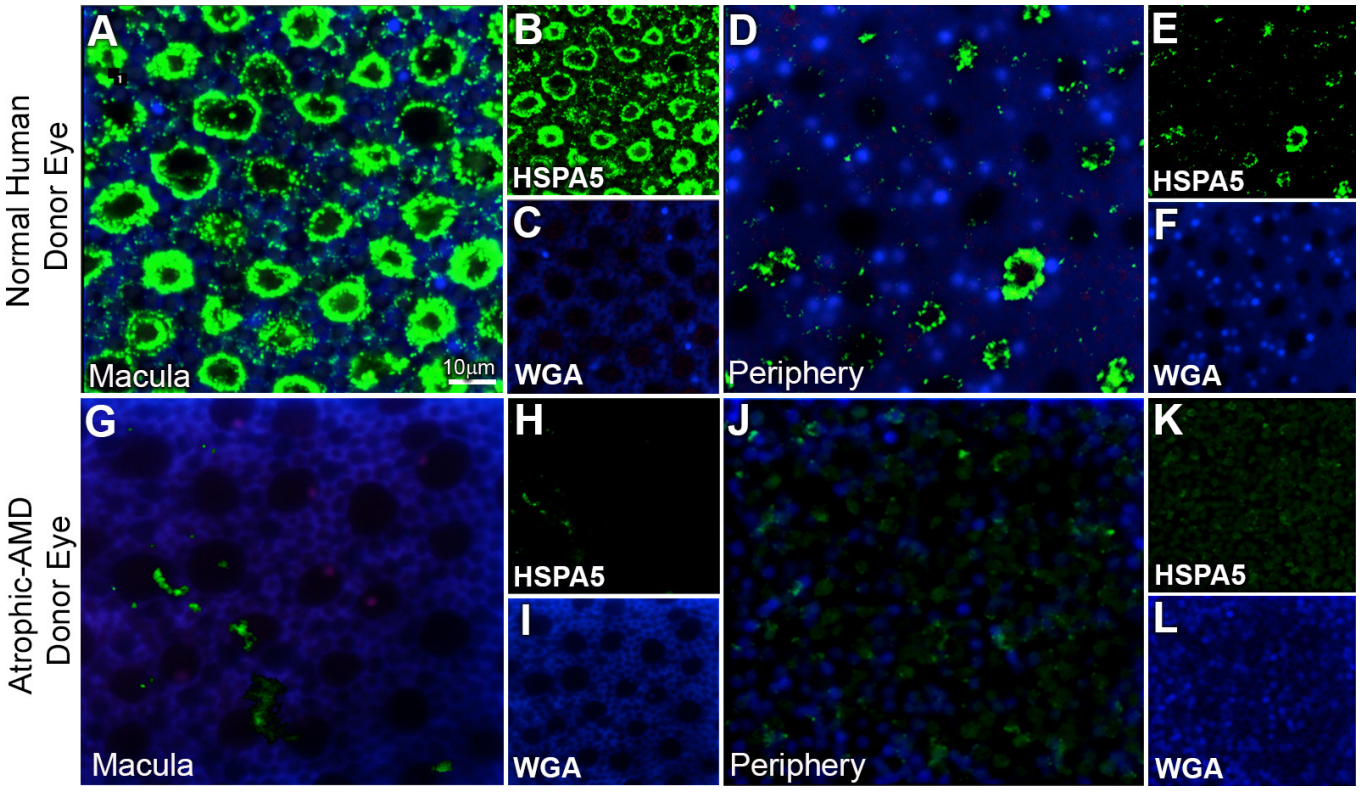

Figure 7. Localization of HSPA5 and WGA in retinas from human donors with no ocular pathology and age-matched donors with diagnosis of atrophic AMD. **A-F**: Localization of HSPA5 and WGA in the retina of a 77-year-old male who had cataract surgery with intraocular lens (IOL) insertion and no history of AMD. **A-C**: In the central macular region of a healthy donor retina, the merged image shows the localization of HSPA5 (green) to the cone IPM in the fovea with lesser labeling around the rod photoreceptors (blue). **D-F**: Merged image of the peripheral retinal area from the same healthy donor demonstrates scattered labeling of HSPA5 (green) on the cone and rod photoreceptors (blue). **G-L**: Localization of HSPA5 and WGA in the retina of a 91-year-old female with dry AMD and bilateral cataracts. **G-I**: Merged image of the central macular region from a dry AMD donor retina shows negligible HSPA5 (green) staining. **J-L**: Merged image of the peripheral retinal area from the same donor with dry AMD shows scattered and unstructured HSPA5 (green) staining. Scale bar = 10 µm. Images are representative of all the donor eyes that were used in the study.

organizing the IPM, which may support photoreceptor function in higher vertebrates. In addition, our data suggested that SULF2 might play a role in modulating HSPA5 expression. This finding can narrow our focus in our attempts to understand the mechanisms of cell-intrinsic programs that alter the IPM. These future outcomes can aid our understanding of why the macula, which is a region rich in cone photoreceptors, is especially vulnerable to photoreceptor degeneration. Our findings provide the first evidence that *Hspa5* may be involved in cone photoreceptor health.

ACKNOWLEDGMENTS

The authors acknowledge the financial support from NEI Grant EY021200, NEI Core Grant P30EY013080, and an unrestricted grant from Research to Prevent Blindness, Inc. We also thank Dr. Eldon Geisert, Dr. Lu Lu, and Mr. Bill Orr for their assistance in generating the BXD microarray datasets that were used in these analyses. The XAP-1 monoclonal antibody (Clone 3D2 developed by D.S. Sakaguchi and W.A. Harris) was obtained from the Developmental Studies Hybridoma Bank, created by the NICHD of the NIH and maintained at The University of Iowa, Department of Biology, Iowa City, IA 52242.

REFERENCES

1. Beere HM, Wolf BB, Cain K, Mosser DD, Mahboubi A, Kuwana T, Tailor P, Morimoto RI, Cohen GM, Green DR. Heat-shock protein 70 inhibits apoptosis by preventing recruitment of procaspase-9 to the Apaf-1 apoptosome. Nat Cell Biol 2000; 2:469-75. .
2. Delpino A, Castelli M. The 78 kDa glucose-regulated protein (GRP78/BIP) is expressed on the cell membrane, is released into cell culture medium and is also present in human peripheral circulation. Biosci Rep 2002; 22:407-20. .
3. Ni M, Zhang Y, Lee AS. Beyond the endoplasmic reticulum: atypical GRP78 in cell viability, signalling and therapeutic targeting. Biochem J 2011; 434:181-8. .
4. Ni M, Lee AS. ER chaperones in mammalian development and human diseases. FEBS Lett 2007; 581:3641-51. .
5. Sun FC, Wei S, Li CW, Chang YS, Chao CC, Lai YK. Localization of GRP78 to mitochondria under the unfolded protein response. Biochem J 2006; 396:31-9. .
6. Yang LP, Wu LM, Guo XJ, Li Y, Tso MO. Endoplasmic reticulum stress is activated in light-induced retinal degeneration. J Neurosci Res 2008; 86:910-9. .
7. Yang LP, Wu LM, Guo XJ, Tso MO. Activation of endoplasmic reticulum stress in degenerating photoreceptors of the rd1 mouse. Invest Ophthalmol Vis Sci 2007; 48:5191-8. .
8. Liu H, Qian J, Wang F, Sun X, Xu X, Xu W, Zhang X, Zhang X. Expression of two endoplasmic reticulum stress markers, GRP78 and GADD153, in rat retinal detachment model and its implication. Eye (Lond) 2010; 24:137-44. .
9. Hauck SM, Schoeffmann S, Deeg CA, Gloeckner CJ, Swiatek-de Lange M, Ueffing M. Proteomic analysis of the porcine interphotoreceptor matrix. Proteomics 2005; 5:3623-36. .
10. Nookala S, Gandrakota R, Wohabrebbi A, Wang X, Howell D, Giorgianni F, Beranova-Giorgianni S, Desiderio DM, Jablonski MM. In search of the identity of the XAP-1 antigen: a protein localized to cone outer segments. Invest Ophthalmol Vis Sci 2010; 51:2736-43. .
11. Wang X, Iannaccone A, Jablonski MM. Permissive glycan support of photoreceptor outer segment assembly occurs via a non-metabolic mechanism. Mol Vis 2003; 9:701-9. .
12. Wohabrebbi A, Umstot ES, Iannaccone A, Desiderio DM, Jablonski MM. Downregulation of a unique photoreceptor protein correlates with improper outer segment assembly. J Neurosci Res 2002; 67:298-308. .
13. Threadgill DW, Miller DR, Churchill GA, de Villena FP. The collaborative cross: a recombinant inbred mouse population for the systems genetic era. ILAR journal / National Research Council Institute of Laboratory Animal Resources 2011; 52:24-31. .
14. Farber CR, Bennett BJ, Orozco L, Zou W, Lira A, Kostem E, Kang HM, Furlotte N, Berberyan A, Ghazalpour A, Suwanwela J, Drake TA, Eskin E, Wang QT, Teitelbaum SL, Lusis AJ. Mouse Genome-Wide Association and Systems Genetics Identify <italic>Asxl2</italic> As a Regulator of Bone Mineral Density and Osteoclastogenesis. PLoS Genet 2011; 7:e1002038-.
15. Hall RA, Liebe R, Hochrath K, Kazakov A, Alberts R, Laufs U, Bohm M, Fischer HP, Williams RW, Schughart K, Weber SN, Lammert F. Systems genetics of liver fibrosis: identification of fibrogenic and expression quantitative trait loci in the BXD murine reference population. PLoS ONE 2014; 9:e89279-.
16. Andreux PA, Williams EG, Koutnikova H, Houtkooper RH, Champy MF, Henry H, Schoonjans K, Williams RW, Auwerx J. Systems genetics of metabolism: the use of the BXD murine reference panel for multiscalar integration of traits. Cell 2012; 150:1287-99. .
17. Taylor BA, Wnek C, Kotlus BS, Roemer N, MacTaggart T, Phillips SJ. Genotyping new BXD recombinant inbred mouse strains and comparison of BXD and consensus maps. Mamm Genome 1999; 10:335-48. .
18. Peirce JL, Lu L, Gu J, Silver LM, Williams RW. A new set of BXD recombinant inbred lines from advanced intercross populations in mice. BMC Genet 2004; 5:7-.
19. Lu H, Li L, Watson ER, Williams RW, Geisert EE, Jablonski MM, Lu L. Complex interactions of Tyrp1 in the eye. Mol Vis 2011; 17:2455-68. .
20. Lu H, Wang X, Pullen M, Guan H, Chen H, Sahu S, Zhang B, Chen H, Williams RW, Geisert EE, Lu L, Jablonski MM. Genetic dissection of the Gpnmb network in the eye. Invest Ophthalmol Vis Sci 2011; 52:4132-42. .

21. Jablonski MM, Freeman NE, Orr WE, Templeton JP, Lu L, Williams RW, Geisert EE. Genetic pathways regulating glutamate levels in retinal Muller cells. Neurochem Res 2011; 36:594-603. .

22. Templeton JP, Freeman NE, Nickerson JM, Jablonski MM, Rex TS, Williams RW, Geisert EE. Innate immune network in the retina activated by optic nerve crush. Invest Ophthalmol Vis Sci 2013; 54:2599-606. .

23. Geisert EE, Lu L, Freeman-Anderson NE, Templeton JP, Nassr M, Wang X, Gu W, Jiao Y, Williams RW. Gene expression in the mouse eye: an online resource for genetics using 103 strains of mice. Mol Vis 2009; 15:1730-63. .

24. Freeman NE, Templeton JP, Orr WE, Lu L, Williams RW, Geisert EE. Genetic networks in the mouse retina: growth associated protein 43 and phosphatase tensin homolog network. Mol Vis 2011; 17:1355-72. .

25. de la Fuente A, Bing N, Hoeschele I, Mendes P. Discovery of meaningful associations in genomic data using partial correlation coefficients. Bioinformatics 2004; 20:3565-74. .

26. Mozhui K, Ciobanu DC, Schikorski T, Wang X, Lu L, Williams RW. Dissection of a QTL hotspot on mouse distal chromosome 1 that modulates neurobehavioral phenotypes and gene expression. PLoS Genet 2008; 4:e1000260-.

27. Mulligan MK, Wang X, Adler AL, Mozhui K, Lu L, Williams RW. Complex control of GABA(A) receptor subunit mRNA expression: variation, covariation, and genetic regulation. PLoS ONE 2012; 7:e34586-.

28. Chintalapudi SM-T. Vanessa; Williams, Robert; Jablonski, Monica. Multipronged Approach to Identify and Validate a Novel Upstream Regulator of Sncg in Mouse Retinal Ganglion Cells (under review). FEBS J 2015; .

29. Bowmaker JK, Dartnall HJ. Visual pigments of rods and cones in a human retina. J Physiol 1980; 298:501-11. .

30. Besharse JC, Pfenninger KH. Membrane assembly in retinal photoreceptors I. Freeze-fracture analysis of cytoplasmic vesicles in relationship to disc assembly. J Cell Biol 1980; 87:451-63. .

31. Libby R, Brunken W, Hunter D. Roles of the Extracellular Matrix in Retinal Development and Maintenance. In: Fini ME, editor. Vertebrate Eye Development. Vol 31: Springer Berlin Heidelberg; 2000. p. 115–40.

32. Johnson LV, Hageman GS, Blanks JC. Interphotoreceptor matrix domains ensheath vertebrate cone photoreceptor cells. Invest Ophthalmol Vis Sci 1986; 27:129-35. .

33. Mieziewska K, van Veen T, Aguirre GD. Structural changes of the interphotoreceptor matrix in an inherited retinal degeneration: a lectin cytochemical study of progressive rod-cone degeneration. Invest Ophthalmol Vis Sci 1993; 34:3056-67. .

34. Ni M, Lee AS. ER chaperones in mammalian development and human diseases. FEBS Lett 2007; 581:3641-51. .

35. Hoozemans JJ, van Haastert ES, Nijholt DA, Rozemuller AJ, Scheper W. Activation of the unfolded protein response is an early event in Alzheimer's and Parkinson's disease. Neurodegener Dis 2012; 10:212-5. .

36. Ghribi O, Herman MM, Pramoonjago P, Savory J. MPP+ induces the endoplasmic reticulum stress response in rabbit brain involving activation of the ATF-6 and NF-kappaB signaling pathways. J Neuropathol Exp Neurol 2003; 62:1144-53. .

37. Sato T, Furukawa K. Transcriptional regulation of the human beta-1,4-galactosyltransferase V gene in cancer cells: essential role of transcription factor Sp1. J Biol Chem 2004; 279:39574-83. .

38. Timpl R, Sasaki T, Kostka G, Chu ML. Fibulins: a versatile family of extracellular matrix proteins. Nat Rev Mol Cell Biol 2003; 4:479-89. .

39. Sethi MK, Buettner FF, Krylov VB, Takeuchi H, Nifantiev NE, Haltiwanger RS, Gerardy-Schahn R, Bakker H. Identification of glycosyltransferase 8 family members as xylosyltransferases acting on O-glucosylated notch epidermal growth factor repeats. J Biol Chem 2010; 285:1582-6. .

40. Veiga-da-Cunha M, Vleugels W, Maliekal P, Matthijs G, Van Schaftingen E. Mammalian phosphomannomutase PMM1 is the brain IMP-sensitive glucose-1,6-bisphosphatase. J Biol Chem 2008; 283:33988-93. .

41. Maeda Y, Tomita S, Watanabe R, Ohishi K, Kinoshita T. DPM2 regulates biosynthesis of dolichol phosphate-mannose in mammalian cells: correct subcellular localization and stabilization of DPM1, and binding of dolichol phosphate. EMBO J 1998; 17:4920-9. .

42. Morava E, Wosik HN, Sykut-Cegielska J, Adamowicz M, Guillard M, Wevers RA, Lefeber DJ, Cruysberg JRM. Ophthalmological abnormalities in children with congenital disorders of glycosylation type I. Br J Ophthalmol 2009; 93:350-4. .

43. Fritsche LG, Chen W, Schu M, Yaspan BL, Yu Y, Thorleifsson G, Zack DJ, Arakawa S, Cipriani V, Ripke S, Igo RP Jr, Buitendijk GH, Sim X, Weeks DE, Guymer RH, Merriam JE, Francis PJ, Hannum G, Agarwal A, Armbrecht AM, Audo I, Aung T, Barile GR, Benchaboune M, Bird AC, Bishop PN, Branham KE, Brooks M, Brucker AJ, Cade WH, Cain MS, Campochiaro PA, Chan CC, Cheng CY, Chew EY, Chin KA, Chowers I, Clayton DG, Cojocaru R, Conley YP, Cornes BK, Daly MJ, Dhillon B, Edwards AO, Evangelou E, Fagerness J, Ferreyra HA, Friedman JS, Geirsdottir A, George RJ, Gieger C, Gupta N, Hagstrom SA, Harding SP, Haritoglou C, Heckenlively JR, Holz FG, Hughes G, Ioannidis JP, Ishibashi T, Joseph P, Jun G, Kamatani Y, Katsanis N, N Keilhauer C, Khan JC, Kim IK, Kiyohara Y, Klein BE, Klein R, Kovach JL, Kozak I, Lee CJ, Lee KE, Lichtner P, Lotery AJ, Meitinger T, Mitchell P, Mohand-Saïd S, Moore AT, Morgan DJ, Morrison MA, Myers CE, Naj AC, Nakamura Y, Okada Y, Orlin A, Ortube MC, Othman MI, Pappas C, Park KH, Pauer GJ, Peachey NS, Poch O, Priya RR, Reynolds R, Richardson AJ, Ripp R, Rudolph G, Ryu E, Sahel JA, Schaumberg DA, Scholl HP, Schwartz SG, Scott WK, Shahid H, Sigurdsson H, Silvestri G, Sivakumaran TA, Smith RT, Sobrin L, Souied EH, Stambolian DE, Stefansson H, Sturgill-Short GM, Takahashi A, Tosakulwong N, Truitt BJ, Tsironi EE, Uitterlinden AG, van Duijn CM, Vijaya L,

Vingerling JR, Vithana EN, Webster AR, Wichmann HE, Winkler TW, Wong TY, Wright AF, Zelenika D, Zhang M, Zhao L, Zhang K, Klein ML, Hageman GS, Lathrop GM, Stefansson K, Allikmets R, Baird PN, Gorin MB, Wang JJ, Klaver CC, Seddon JM, Pericak-Vance MA, Iyengar SK, Yates JR, Swaroop A, Weber BH, Kubo M, Deangelis MM, Léveillard T, Thorsteinsdottir U, Haines JL, Farrer LA, Heid IM, Abecasis GR; AMD Gene Consortium. Seven new loci associated with age-related macular degeneration. Nat Genet. 2013;45:433-9, 439e1-2.

44. Dhoot GK, Gustafsson MK, Ai X, Sun W, Standiford DM, Emerson CP Jr. Regulation of Wnt signaling and embryo patterning by an extracellular sulfatase. Science (New York, NY) 2001; 293:1663-6. .

45. Ai X, Kitazawa T, Do AT, Kusche-Gullberg M, Labosky PA, Emerson CP Jr. SULF1 and SULF2 regulate heparan sulfate-mediated GDNF signaling for esophageal innervation. Development 2007; 134:3327-38. .

46. Danesin C, Agius E, Escalas N, Ai X, Emerson C, Cochard P, Soula C. Ventral neural progenitors switch toward an oligodendroglial fate in response to increased Sonic hedgehog (Shh) activity: involvement of Sulfatase 1 in modulating Shh signaling in the ventral spinal cord. J Neurosci 2006; 26:5037-48. .

47. Fujita K, Takechi E, Sakamoto N, Sumiyoshi N, Izumi S, Miyamoto T, Matsuura S, Tsurugaya T, Akasaka K, Yamamoto T. HpSulf, a heparan sulfate 6-O-endosulfatase, is involved in the regulation of VEGF signaling during sea urchin development. Mech Dev 2010; 127:235-45. .

48. Gallagher JT. Heparan sulfate: growth control with a restricted sequence menu. J Clin Invest 2001; 108:357-61. .

49. Viviano BL, Paine-Saunders S, Gasiunas N, Gallagher J, Saunders S. Domain-specific modification of heparan sulfate by Qsulf1 modulates the binding of the bone morphogenetic protein antagonist Noggin. J Biol Chem 2004; 279:5604-11. .

Articles are provided courtesy of Emory University and the Zhongshan Ophthalmic Center, Sun Yat-sen University, P.R. China. The print version of this article was created on 10 November 2016. This reflects all typographical corrections and errata to the article through that date. Details of any changes may be found in the online version of the article.